

# Observation of a controllable $\pi$ -junction in a 3-terminal Josephson device

Jian Huang<sup>1</sup>, F. Pierre<sup>1</sup>, Tero T. Heikkilä<sup>2</sup>, Frank K. Wilhelm<sup>3</sup>, and Norman O. Birge<sup>1</sup>

<sup>1</sup> Department of Physics and Astronomy, Michigan State University, East Lansing, MI 48824-1116

<sup>2</sup> Materials Physics Laboratory, Helsinki University of Technology, FIN-02015 HUT, Finland

<sup>3</sup> Sektion Physik und CeNS, LMU, Theresienstr. 37, D-80333 München, Germany

(January 7, 2002)

Recently Baselmans et al. [Nature, 397, 43, (1999)] showed that the direction of the supercurrent in a superconductor/normal/superconductor Josephson junction can be reversed by applying, perpendicularly to the supercurrent, a sufficiently large control current between two normal reservoirs. The novel behavior of their 4-terminal device (called a controllable  $\pi$ -junction) arises from the nonequilibrium electron energy distribution established in the normal wire between the two superconductors. We have observed a similar supercurrent reversal in a 3-terminal device, where the control current passes from a single normal reservoir into the two superconductors. We show theoretically that this behavior, although intuitively less obvious, arises from the same nonequilibrium physics present in the 4-terminal device. Moreover, we argue that the amplitude of the  $\pi$ -state critical current should be at least as large in the 3-terminal device as in a comparable 4-terminal device.

74.50.+x, 73.23.-b, 85.25.Am, 85.25.Cp

When a normal metal is put in contact with one or more superconductors, the properties of both materials are modified near the interface. The physical phenomena associated with superconductor (S)/normal (N) systems, namely the proximity and Josephson effects, were intensely studied in the 1960's and 70's.<sup>1</sup> Interest in S/N systems was rekindled in the 1990's due to the ability to fabricate complex structures with submicrometer dimensions. A new, deeper understanding of the proximity effect on mesoscopic length scales has emerged,<sup>2,3</sup> concentrating on equilibrium and linear-response physics.

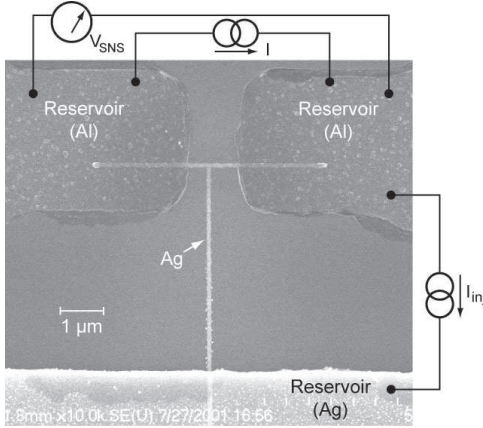


FIG. 1. Scanning electron microscope picture of the sample, with schematic drawing of the measurement circuit. The sample consists of a T-shaped Ag wire with lateral dimensions of 50 nm  $\times$  70 nm, connected to two 70 nm thick Al electrodes and one 230 nm thick Ag electrode.

Nonequilibrium phenomena in S/N systems are now taking the spotlight.<sup>4,6</sup> A major discovery was made by Baselmans et al.,<sup>6</sup> who measured a 4-terminal diusive metal S/N/S Josephson device with a cross shape. Two

opposing ends of the cross were connected to S electrodes, while the other two were connected to N reservoirs between which a control current was passed. Baselmans et al. found that, at high control current, in samples with the normal reservoirs sufficiently close together, the sign of the Josephson supercurrent between the S electrodes reversed direction. The current-phase relationship under such conditions becomes  $I_s(\phi) = I_c \sin(\phi + \pi)$ ; where  $I_c$  is the (positive) critical supercurrent, rather than the usual Josephson relationship  $I_s(\phi) = I_c \sin(\phi)$ , hence the device is called a  $\pi$ -junction. Such a device has been used to make a controllable  $\pi$ -SQUID.<sup>7</sup> The explanation of the nonequilibrium  $\pi$ -junction consists of two parts.<sup>8</sup> First, the supercurrent can be decomposed into an energy-dependent "spectral supercurrent"  $j_E$ , which is an equilibrium property determined by the sample geometry and resistance as well as the phase difference between the two S electrodes.  $j_E$  is an odd function of energy, and exhibits damped oscillations on an energy scale comparable to the Thouless energy of the sample,  $E_{th} = \hbar D/L^2$ ; with  $D$  the diffusion constant in the wire and  $L$  the length between the superconductors. Second, the total supercurrent is determined by the occupation of the supercurrent-carrying states, given by the antisymmetric part of the quasiparticle distribution function  $f(E)$  in the normal region of the junction describing the pairs of quasiparticles ( $E > E_F$ ) and quasiholes ( $E < E_F$ ). Under nonequilibrium conditions,  $f(E)$  can be made to have a staircase shape, with steps appearing at the voltages of the normal reservoirs.<sup>10</sup> The staircase shape of  $f(E)$  excludes the low-energy contribution of  $j_E$  from the supercurrent. When the control voltage approaches the energy where  $j_E$  changes sign, the supercurrent changes its sign relative to the equilibrium situation. In contrast to the  $\pi$ -junction behavior, smearing of the distribution function by electron heating or raising the sample temperature simply causes the supercurrent to decrease toward zero without ever changing sign.

The sample shown in Fig. 1 consists of a T-shaped Ag wire, 70 nm wide and 50 nm thick, connected to two S

electrodes (70 nm of Ag) and one N reservoir (230 nm of Ag). The distance between S electrodes is 1.1  $\mu\text{m}$ , while the distance from the top of the "T" to the N reservoir is 4.5  $\mu\text{m}$ . The phase coherence length  $L$  in similarly prepared Ag wires is several micrometers at sub-Kelvin temperatures, hence we expect to observe a substantial Josephson effect between the two S electrodes. The sample was fabricated using one electron-beam and two optical lithography steps. The T-shaped Ag wire was fabricated first, followed by the thick Ag reservoir, and finally the Al electrodes. A gentle ion mill of the exposed ends of the Ag wire preceded the evaporation of the Al electrodes to enhance the transparency of the Ag/Al interfaces. The sample was immersed in the mixing chamber of a dilution refrigerator with filtered electrical leads.

The transport properties of the sample were determined initially by measuring the  $V$  vs.  $I$  characteristics between pairs of electrodes. The  $V$ - $I$  curve between S electrodes shows the standard Josephson junction behavior with a critical current of 0.7  $\mu\text{A}$  at 38 mK. The  $V$ - $I$  curve between the N electrode and either S electrode exhibits a change in slope at a current approximately equal to twice the critical current. This behavior is due to the superposition of opposite-flowing quasiparticle current and supercurrent in the dangling arm, as observed recently by Shaikhaidarov et al.<sup>11</sup>. For the sample shown in Fig. 1, the left and right arm have resistances of  $R_1 = 7.0$  and  $R_2 = 9.1$   $\Omega$ , respectively, while the base of the T has a resistance of  $R_0 = 36$   $\Omega$ . From these values and the sample geometry, we deduce that about half of the 16.1  $\Omega$  S-S resistance comes from the uncovered part of the Ag wire, and the other half from the Al/Ag interfaces and part of the Ag wire extending under the Al electrodes.

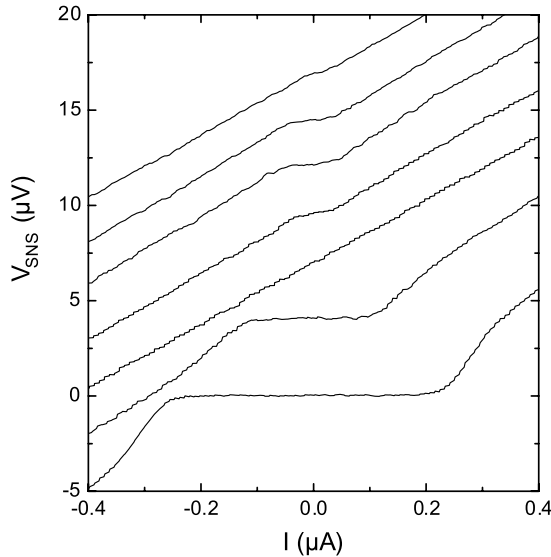


FIG. 2. A subset of  $V_{\text{SNS}}$  vs.  $I$  curves measured across the S/N/S Josephson junction, for different values of the current injected from the normal reservoir. From bottom to top, the injected currents  $I_{\text{inj}}$  are in  $\mu\text{A}$ : 0.53, 0.70, 1.01, 1.23, 1.89, 2.18, 3.15. The curves are offset for clarity.

The measurement circuit for the nonequilibrium injection experiment is shown schematically in Fig. 1. A dc current  $I_{\text{inj}}$  is injected from the normal electrode to one of the superconducting electrodes. Simultaneously, the  $V$ - $I$  curve between the two superconducting electrodes is measured in a 4-probe configuration. Figure 2 shows a subset of  $V$ - $I$  curves for different values of  $I_{\text{inj}}$ , and is the central result of this paper. The critical current of the S/N/S junction decreases rapidly with increasing injection current. When  $I_{\text{inj}} = 1.0$   $\mu\text{A}$ , the critical current is below our measurement threshold. Upon further increase of  $I_{\text{inj}}$ , the critical current increases again, and finally disappears when  $I_{\text{inj}} > 3$   $\mu\text{A}$ . In Figure 3, we plot  $I_c$  vs.  $V_N$  at three different temperatures, where  $V_N = R_N I_{\text{inj}}$  is the voltage of the normal reservoir with respect to the superconductors, and  $R_N = R_0 + (R_1^{-1} + R_2^{-1})^{-1} = 40$   $\Omega$ . In the figure we intentionally plot  $I_c < 0$  after it falls to zero, to emphasize that the junction has entered the " state.<sup>12</sup> Our interpretation of the data is consistent with the assumption that, for fixed  $I_{\text{inj}}$ ,  $I_s$  is a smooth function of  $V_N$  with a continuous first derivative. It is also consistent with the experiment of Baselmans et al.,<sup>6</sup> who confirmed the existence of the " state by measuring the resistance of the normal wire as a function of the supercurrent, hence the phase difference  $\phi$ , between the S electrodes. At zero supercurrent, their wire resistance exhibits a local minimum in the usual "0" state and a local maximum in the " state due to the proximity effect.

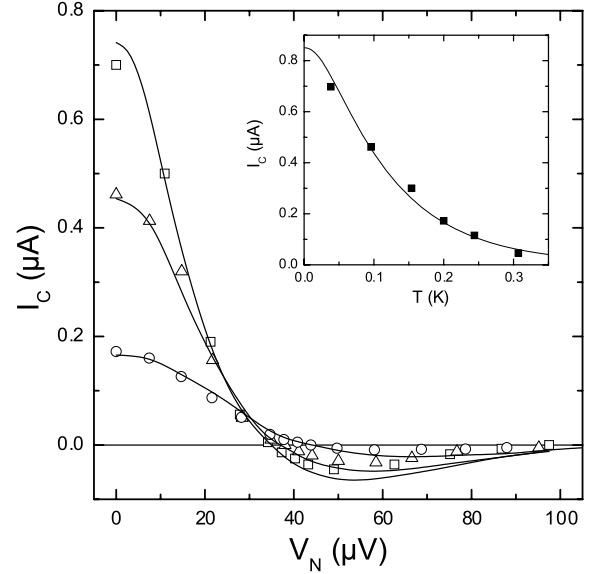


FIG. 3. Critical current of the Josephson junction vs. voltage of the normal reservoir at  $T = 38$  ( $\square$ ),  $96$  ( $\triangle$ ) and  $200$  mK ( $\circ$ ).  $I_c$  is shown as negative for  $V_N > 40$   $\mu\text{V}$  to symbolize the appearance of the " junction. Inset: Critical current vs. temperature at  $V_N = 0$ . The lines are the theoretical calculations discussed in the text.

The significant difference between our experiment and that of Baselmans et al., aside from the reduction from 4 terminals to 3, is the presence in our sample of a dissi-

pative quasiparticle current in the sample arms that simultaneously carry the supercurrent. In the Basel experiment, the control voltages of the two normal reservoirs were set to values  $V_N$  with respect to the superconductors, so that the electrical potential was zero everywhere along the wire connecting the two superconductors. To compare our experiment with theirs, we must understand the influence of the dissipative current on the supercurrent in our sample. We use the quasiclassical formalism in real time, which was originally developed for nonequilibrium phenomena in massive superconductors<sup>13</sup> but also adapted and successfully applied to mesoscopic proximity systems, as reviewed e.g. in refs. 3 and 14.

For the present paper, we are concerned primarily with the supercurrent

$$I_S = \frac{N A}{2} \int_{-Z}^Z j_E f_L(E) dE; \quad (1)$$

where  $N$  and  $A$  are the conductance and cross-section of the normal wire,  $j_E$  is the spectral supercurrent discussed earlier, and  $f_L(E) = f(E) - f(E)$  is the antisymmetric part of the electron energy distribution function. With the chemical potential of the superconductors taken to be zero, the symmetric distribution function  $f_T(E) = 1 - f(E) - f(E)$  describes charge in balance, while  $f_L(E)$  describes energy or heat in the conduction electron system.

To calculate the supercurrent, first one must solve the Usadel equation for the retarded and advanced Green's functions. Those contain all information about energy-dependent properties of the sample, including the function  $j_E$ . To find  $f_L(E)$ , one must then solve the Keldysh component of the Usadel equation, which takes the form of conservation laws for the spectral charge and heat currents.<sup>14</sup> When  $j_E \neq 0$ , the two kinetic equations are coupled, and lead to complicated spatial and energy dependences of  $f_L(E)$  and  $f_T(E)$  in the arms of the sample between the superconductors. A major simplification occurs in the arm of the sample connected to the normal reservoir:  $j_E = 0$  there since the superconducting phase is constant along that arm. For voltages and temperatures small compared to the heat current is zero,<sup>15</sup> hence  $f_L(E)$  is constant along that arm and takes on the (equilibrium) value it has in the  $N$  reservoir:  $f_L^0 = (1/2)f \tanh[(E + eV_N)/2k_B T] + \tanh[(E - eV_N)/2k_B T]g$ . Since the total charge current is conserved along the two sample arms connecting the superconductors, we can evaluate it anywhere in those arms. At the central point, the dissipative currents diverted into the two arms cancel and we can find the supercurrent from Eq. (1) using the expression for  $f_L^0(E)$  given above, without integrating the kinetic equations. We need only to evaluate  $j_E$  at the central point by solving the equilibrium Usadel equation for our sample geometry.

As an extension of previous work,<sup>9</sup> we have solved the retarded Usadel equation taking into account the influence of the lead to the normal reservoir and the finite

interface resistances.<sup>16</sup> The normal reservoir induces extra decoherence into the structure, decreasing the magnitude of the observed supercurrent. We find that the full gap in the spectral supercurrent<sup>9</sup> becomes a pseudogap and that the amplitude of the maximum of  $j_E$  is strongly reduced (although the total supercurrent is reduced by only 20% at 40 mK). Our fit to the equilibrium data of critical supercurrent vs. temperature is shown in the inset to Figure 3. To fit the temperature dependence, the Thouless energy was adjusted to be  $E_{Th} = 3.5$  eV, which corresponds to a distance  $L = 1.7$   $\mu$ m between the superconducting electrodes (larger than the actual distance as a result of the silver wire penetration under the aluminium reservoirs and of the finite contact resistances). Surprisingly, the magnitude of the calculated critical current had to be reduced by a factor 1.7 to match the experimental data, possibly due to the rather high S/N interface resistances in this sample.<sup>17</sup>

If we now calculate the nonequilibrium data of  $I_c$  vs.  $V_N$  using the equilibrium form for  $f_L^0$  in the normal reservoir, we find that the calculation overestimates the critical current in the  $\backslash$  state by a large factor, and predicts too small a voltage at which the supercurrent changes sign. This failure results from neglecting inelastic collisions inside the wire and electron heating in the normal reservoir. Based on our previous measurements of  $f(E)$  in nonequilibrium mesoscopic metal wires,<sup>10,18</sup> we can estimate the contributions of both inelastic scattering and reservoir heating to the rounding of  $f(E)$  in our sample. Inelastic scattering in similar Ag wires was well described within the framework of the Boltzmann equation using an electron-electron interaction kernel in agreement with the theoretical form  $K(E) = K_{3=2} E^{-3=2}$ ; but with a prefactor  $K_{3=2} = 0.5 \text{ ns}^{-1} \text{ m eV}^{-1=2}$ , about 5 times larger than predicted by theory. Heating of the normal reservoir can be estimated using the Wiedemann-Franz law and a simplified model of electron-phonon scattering in the reservoir.<sup>19,20</sup> The temperature of the electrons in the reservoir is given by  $T_e = \sqrt{T^2 + b^2 V_N^2}$  where  $b^2$  is proportional to the ratio of the reservoir sheet resistance to the wire resistance.<sup>19</sup> From our sample parameters and previous measurements of similar samples,<sup>20</sup> we estimate  $b = 1 \text{ K/mV}$ . Using these values of  $K_{3=2}$  and  $b$ , we have calculated  $f(E)$  and thereby  $I_c(V_N)$  in our sample by solving the Boltzmann equation with the correct boundary conditions at the S/N interfaces,<sup>5</sup> but neglecting proximity effect in the bulk of the wire. The result of that calculation does not fit the data shown in Fig. 3. A much larger value of  $K_{3=2} = 3 \text{ ns}^{-1} \text{ m eV}^{-1=2}$  provides a reasonable fit, but leaves us without a plausible explanation for the enhanced electron-electron interactions. An alternative approach is to use an interaction kernel of the form  $K(E) = K_2 E^{-2}$ , which describes samples containing dilute magnetic impurities.<sup>20,21</sup> With the value  $K_2 = 0.55 \text{ ns}^{-1}$ , corresponding to a magnetic impurity concentration of about 0.1 ppm, we obtain the solid curves shown in Fig. 3, which fit the data well at voltages

up to the crossover to the junction. Adding a reasonable  $K_{3=2}$  term to  $K(E)$  improves the fit only slightly at higher voltages. The magnetic impurity concentration of 0.1 ppm is plausible, and will limit  $L$  to about 5 nm near the Kondo temperature (still much larger than the distance between the two superconducting electrodes).

The rather poor fit to the data at high voltages may reflect the fact that the magnitude of  $I_c$  in the state depends on a delicate balance between the positive and negative parts of  $j_E$ , weighted by the precise shape of  $f(E)$ : Fig. 4 shows  $f(E)$  for  $V_N = 50$  V, near the maximum junction  $I_c$ . By eye  $f(E)$  looks nearly like a hot Fermi-Dirac function, but the dashed line in the figure shows that it is not. If the sample were shorter, so that  $f(E)$  maintained the staircase structure of the dotted line in the figure, the junction  $I_c$  would be much larger.

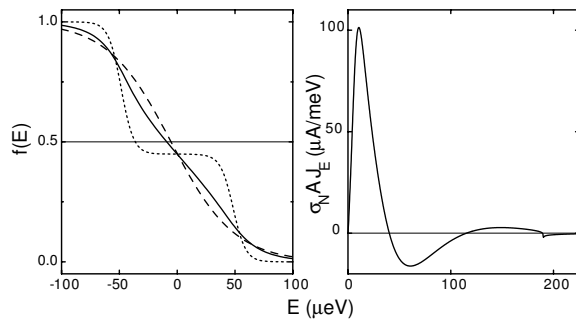


FIG. 4. Left: Solid line: distribution function  $f(E)$  used to calculate the Josephson junction current in the state at  $V_N = 50$  V and  $T = 38$  mK. Dotted line:  $f(E)$  taking into account only reservoir heating but not energy exchange. Dashed line: hot Fermi-Dirac distribution. Right: Numerically calculated  $j_E$  (multiplied by the prefactor  $N_A$ ), at the central point of the sample, shown only for  $E > 0$ .

Fig. 4 also reveals the difference between our 3-terminal experiment and the 4-terminal experiment of Baselmans et al. In our sample the electrical potential is nonzero at the central point, since the injection current flows into both S electrodes. Hence  $f(E=0) \neq \frac{1}{2}$  at the central point, unlike in Baselmans' sample. (The deviation from  $1/2$  is small, since the vertical arm of our sample is much longer than the horizontal arms.) Since the available phase space for quasiparticle energy exchange decreases as  $f(E)$  deviates from  $1/2$ , the 3-terminal geometry should be favorable for maximizing  $I_c$  in the state. A direct measurement of this subtle effect could be made in a 4-terminal sample. Biasing the two normal reservoirs at the same potential  $V_N$ , rather than at asymmetric voltages  $V_N$ , would result in a current flow pattern and distribution functions essentially equivalent to those in our 3-terminal experiment. A comparison of the values of  $I_c$  in the state under symmetric bias ( $V_N; V_N$ ) and antisymmetric bias ( $V_N; -V_N$ ) might reveal a subtle difference in the smearing of  $f(E)$ . We plan to explore this comparison experimentally.

We thank D. Esteve and H. Pothier for suggesting the "dangling arm" experiment, and I.O. Kulik for a valuable discussion concerning electron heating. This work was supported by NSF grants DMR-9801841 and 0104178, and by the Keck Microfabrication Facility supported by NSF DMR-9809688.

- <sup>1</sup> G. Deutscher and P.G. deGennes, in *Superconductivity*, edited by R.D. Parks (Marcel Dekker, New York, 1969), p. 1005; K.K. Likharev, *Rev. Mod. Phys.* 51, 101 (1979).
- <sup>2</sup> B. Pannetier and H. Courtois, *J. Low Temp. Phys.* 188, 599 (2000), and references therein.
- <sup>3</sup> C.J. Lambert and R. Raimondi, *J. Phys.: Condens. Matter* 10, 901 (1998).
- <sup>4</sup> Th. Schapers et al., *Appl. Phys. Lett.* 73, 2348 (1998).
- <sup>5</sup> F. Pierre et al., *Phys. Rev. Lett.* 86, 1078 (2001).
- <sup>6</sup> J.J.A. Baselmans et al., *Nature* 397, 43 (1999) and *Phys. Rev. B* 63, 094504 (2001).
- <sup>7</sup> J.J.A. Baselmans, B.J. van Wees, and T.M. Klapwijk, *Appl. Phys. Lett.* 79, 2940 (2001).
- <sup>8</sup> B.J. van Wees, K.M.H. Lenssen and C.J.P.M. Harmans, *Phys. Rev. B* 44, 470 (1991); G. Wendin and V.S. Shumeiko, *Phys. Rev. B* 53, R6006 (1996); L.-F. Chang and P.F. Bagwell, *Phys. Rev. B* 55, 12678 (1997).
- <sup>9</sup> F.K. Wilhelm, G. Schon and A.D. Zaikin, *Phys. Rev. Lett.* 81, 1682 (1998); S.-K. Yip, *Phys. Rev. B* 58, 5803 (1998).
- <sup>10</sup> H. Pothier et al., *Phys. Rev. Lett.* 79, 3490 (1997).
- <sup>11</sup> R. Shaikhaidarov et al., *Phys. Rev. B* 62, R14649 (2000).
- <sup>12</sup> Technically it is not correct to say that  $I_c$  changes sign. What changes sign is  $I_s(\phi)$  for a fixed value of  $\phi$ , e.g.  $\phi = \pi$ . Hence  $I_c$  stays positive when  $V_N$  exceeds 40 V, while  $I_s$  changes from  $I_c \sin(\phi)$  to  $I_c \sin(\phi + \pi)$ .
- <sup>13</sup> J. Rammer and H. Smith, *Rev. Mod. Phys.* 58, 323 (1986).
- <sup>14</sup> W. Belzig et al., *Superlattices Microstruct.* 25, 1251 (1999). The kinetic equations are valid in a normal metal without inelastic scattering.
- <sup>15</sup> A.F. Andreev, *Sov. Phys. JETP* 19, 1228 (1964).
- <sup>16</sup> W. Belzig et al., *Phys. Rev. B* 62, 9726 (2000); K.M. Schep and G.E.W. Bauer, *Phys. Rev. Lett.* 78, 3015 (1997).
- <sup>17</sup> In a private communication, J.J.A. Baselmans told us that similarly prepared samples can show large variations in the overall magnitude of the supercurrent while the function dependence on the voltage remains the same.
- <sup>18</sup> F. Pierre et al., *J. Low Temp. Phys.* 118, 437 (2000).
- <sup>19</sup> M. Henny et al., *Phys. Rev. B* 59, 2871 (1999).
- <sup>20</sup> F. Pierre et al., in *Kondo Effect and Dephasing in Low-Dimensional Metallic Systems*, Ed. V. Chandrasekhar, C. Van Haesendonck, and A. Zawadowski, (Kluwer, Dordrecht, 2001), p. 119 (e-print: cond-mat/0012038); F. Pierre, *Ann. Phys. Fr.* 26 N 4 (2001).
- <sup>21</sup> A. Kaminski and L.J. Glazman, *Phys. Rev. Lett.* 86, 2400 (2001).